Quadruply resonant optical parametric oscillation in a monolithic total-internal-reflection resonator

S. Schiller* and R. L. Byer

Department of Applied Physics, Stanford University, Stanford, California 94305

Received March 18, 1993

Monolithic total-internal-reflection resonators are low-loss broadband devices that permit variable input–output coupling. They are ideally suited as resonators for high-efficiency low-threshold widely tunable continuous-wave optical parametric oscillation. We demonstrate a continuous-wave quadruply resonant MgO:$LiNbO_3$ optical parametric oscillator in which doubly resonant second-harmonic generation and doubly resonant optical parametric oscillation occur simultaneously. The threshold subharmonic power at 1.06 μm for oscillation near 1.06 μm is 0.4 mW. Stable single-frequency operation is achieved, and the tuning curve is measured.

1. INTRODUCTION

Significant improvements in the performance of cw optical parametric oscillators (OPO's) have taken place in the past few years, partly because of the use of single-frequency low-amplitude-noise pump lasers and novel OPO cavity designs and partly because of improved nonlinear crystals. The combination of a monolithic design for OPO cavities,[1] which are inherently mechanically stable and low loss because of the absence of intracavity interfaces, and diode-laser-pumped solid-state lasers has led to doubly resonant OPO's (DRO's) with thresholds of the order of 10 mW, whose output is stable in frequency and power.[2]

We describe here what is to our knowledge the first application of a novel type of optical resonator, the monolithic total-internal-reflection resonator (MOTIRR),[3] to nonlinear optics, demonstrating simultaneous second-harmonic generation (SHG) and parametric oscillation.

In a MOTIRR the modes are confined by total internal reflection (TIR), and input–output coupling is achieved by frustrated TIR (FTIR) at one of the facets of the resonator. The elimination of dielectric coatings and the use of easily variable input–output coupling offer significant advantages compared with previous monolithic resonators. These advantages are as follows:

(1) Resonator losses that are due to reflection losses are minimized, since a well-polished and clean TIR face has near-unity reflectivity, which is ultimately limited by the surface roughness.[4] A rms roughness of <5 nm yields a TIR scatter loss of <0.1% for a wavelength of 1 μm or longer. Such smoothness can be readily achieved.[5] A $LiNbO_3$ MOTIRR, described below, exhibited a total (bulk plus surface) loss of 0.2% at 1 μm. This represents the lowest value in a bulk nonlinear resonator demonstrated to date.

(2) MOTIRR's are broadband and are therefore ideally suited for applications that require simultaneous resonance of widely different wavelengths. Examples are doubly resonant (DR) SHG, in which the subharmonic and harmonic waves are both resonant with cavity modes, and nondegenerate DR parametric oscillation.

(3) The permitted temperature operating range is not limited by potential damage to coatings. With the appropriate crystals, phase matching over an extended wavelength range by temperature-tuned noncritical phase matching is possible. SHG with tunable sources and widely tunable parametric oscillation with fixed-wavelength pumps become possible by use of MOTIRR devices.

(4) Optimizable input coupling permits maximally efficient frequency conversion at any power level. The efficiencies of frequency-conversion processes depend on cavity loss and input mirror transmission of the external pump wave. Typically, the efficiency can be maximized with respect to the input mirror transmission. For singly resonant (SR) and DR SHG, this procedure is equivalent to impedance matching, i.e., the equalization of input coupler transmission and internal pump losses (absorption, scatter, and conversion). In MOTIRR's one can manually find optimum coupling values easily and quickly at an arbitrary power level by changing the strength of FTIR, whereas conventional resonators require that one have prior knowledge of losses and single-pass conversion efficiency to determine optimum coating reflectivities for a single input power value. Individual FTIR coupling control for different wavelengths is possible if a respective number of coupling prisms of birefringent and/or dispersive materials is used to provide polarization and/or wavelength-selective FTIR transmissions.[6,7]

Relatively few experimental realizations of cw frequency conversion in cavities resonant at widely different wavelengths have been reported in spite of the fundamental importance of such processes. DR SHG, for example, represents a paradigm of physics, a system of two harmonic oscillators coupled by a nonlinear interaction and driven by an external force, and has been predicted to exhibit rich nonlinear dynamics.[8,9] In addition, DR SHG can generate nonclassical light.[10–14] Practical applications of DR SHG for spectroscopic uses[15,16] stem from the fact that it is more efficient than SHG in which either the subharmonic or the harmonic wave is resonated.

The potential of lowering the OPO threshold by resonating not only signal and idler but also the pump wave in a

0740-3224/93/091696-12$06.00

triply resonant OPO (TRO) was theoretically analyzed early on.[17] KTP[18] and lithium borate[19] TRO's with pump-frequency finesses of 25 and 6, respectively, were recently operated. In this paper we show that, near degeneracy, the subharmonic power required for reaching threshold of a quadruply resonant OPO (QRO), in which the subharmonic of the (resonant) pump wave is also resonated, is approximately twice as large as the threshold of a TRO at the harmonic frequency. The QRO threshold is $2a_2$ times smaller than the DRO threshold, where a_2 is the cavity loss at the harmonic frequency. Since DRO thresholds of the order of 10 mW have been demonstrated,[2] TRO's or QRO's can reduce thresholds below the milliwatt level. We reached this level in the present study by using a monolithic ring resonator whose losses (harmonic finesse $\approx$200, subharmonic finesse $\approx$750) are lower than those of any previously described multiply resonant device.

This paper is structured as follows. The theory of DR SHG is summarized in Section 2. DR SHG requires that the laser frequency and its harmonic lie within the bandwidth of cavity resonances. The use of laser frequency and MOTIRR temperature as tuning parameters is discussed in Subsection 2.A. The formulas for the calculation of intracavity subharmonic and harmonic powers are given in Subsection 2.B. A generalization of the Boyd–Kleinman focusing factor is presented in Subsection 2.C, which takes into account astigmatism and SHG interference effects. The threshold for quadruply resonant parametric oscillation and the structure of the output spectrum are derived in Subsections 3.A and 3.B, respectively. In Subsection 4.A we describe two $LiNbO_3$ MOTIRR's and some details of the setup. MOTIRR characterization procedures are discussed in Subsection 4.B. Parametric oscillation results are given in Subsection 4.C.

2. DOUBLY RESONANT SECOND-HARMONIC GENERATION

A. Tuning

We consider a $LiNbO_3$ monolithic ring resonator with the crystal c axis normal to the ring plane, as depicted in Fig. 1. In a uniaxial crystal this orientation avoids bireflection effects and leads to identical wavelength-independent ring paths for both the ordinary and the extraordinary polarizations. Type-I noncritically phase-matched SHG, with a p-polarized (ordinary) subharmonic wave and an s-polarized (extraordinary) harmonic wave, can thus occur along the whole ring. Mode overlap is complete for TEM_{00} subharmonic and harmonic waves.

Double-resonance of subharmonic and harmonic waves is achieved when the following conditions for the round-trip phase changes are simultaneously satisfied:

$$\frac{n_o(\omega_1)\omega_1 L_{rt}}{c} - \phi_x - \phi_y + \sum_{j=1}^{N} \gamma_p^{(j)} = 2\pi M_1, \tag{1}$$

$$\frac{n_e(2\omega_1)2\omega_1 L_{rt}}{c} - \phi_x - \phi_y + \sum_{j=1}^{N} \gamma_s^{(j)} = 2\pi M_2. \tag{2}$$

Here L_{rt} is the ring length; the sum is over all N reflections of the ring cavity; $\gamma_s^{(j)}$, $\gamma_p^{(j)}$ are TIR phase shifts for the s-polarized harmonic and the p-polarized subharmonic waves, respectively, at face j, defined in Ref. 3; M_i are integer mode numbers; ϕ_x, ϕ_y are the mode-dependent Guoy phase shifts[20]; and n_o and n_e are the ordinary and the extraordinary indices of refraction, respectively. In an astigmatic resonator, which is the case for a MOTIRR with a single spherically polished facet, the TEM_{00} mode has an elliptical cross section, with in-plane (tangential) and out-of-plane (sagittal) waists given, respectively, by

$$w_x^2 = \frac{\lambda_0 L_{rt}}{2\pi n}\left(\frac{2R\cos\theta}{L_{rt}} - 1\right)^{1/2},$$

$$w_y^2 = \frac{\lambda_0 L_{rt}}{2\pi n}\left(\frac{2R}{L_{rt}\cos\theta} - 1\right)^{1/2}, \tag{3}$$

where λ_0 is the vacuum wavelength of the mode, θ is the angle of incidence onto the curved face, and $n = n(\lambda_0)$ is the resonator index. Introducing the ellipticity parameter $\alpha = w_x/w_y$, and the Rayleigh range $z_r = k_1 w_{1x} w_{1y}/2$ (k_i are the wave numbers), we can express the Guoy phase shifts for TEM_{00} modes by the equations

$$\phi_x = \arctan\left(\frac{L_{rt}}{2\alpha z_r}\right), \qquad \phi_y = \arctan\left(\frac{L_{rt}\alpha}{2z_r}\right). \tag{4}$$

Experimentally, the subharmonic resonance condition [Eq. (1)] is readily satisfied when one uses a servo system to control the laser frequency. In this situation the resonance condition for the harmonic wave can be rewritten as

$$\Delta k L_{rt} + \phi_x + \phi_y + \sum_{j=1}^{N} \gamma_s^{(j)} - 2\gamma_p^{(j)} = 2\pi m, \tag{5}$$

where $\Delta k = k_2 - 2k_1$ is the wave-vector mismatch and m is an integer. Subsequent double resonances (implying a change in mode number M_2 of the harmonic by 1 if the subharmonic is kept frequency locked to a particular mode number) require a change in the round-trip wave-vector mismatch $\Delta k L_{rt}$ by 2π.

Tuning to obtain double resonance thus requires an external agent that modifies the value of $\Delta k L_{rt}$. Since, for efficient phase matching and conversion, the resonator must be operated at values of $\Delta k L_{rt}$ of the order of unity, changes in round-trip length L_{rt} of the order of micrometers do not contribute significantly to a change in $\Delta k L_{rt}$.

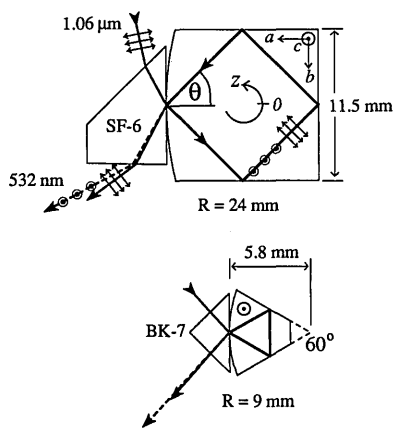

Fig. 1. Geometries of $LiNbO_3$ MOTIRR's. The beam waists are located opposite the curved face. The short flat face of the triangular MOTIRR is polished for alignment and for gap-monitoring purposes. SF-6, BK-7, coupling prism materials.

The wave-vector mismatch Δk can be tuned by temperature, electric field,[21] or strain,[14] through the thermal sensitivity of the birefringence, the electro-optic effect, or the elasto-optic effect, respectively. An electric field is the most practical tuning parameter, being simple to implement and fast. However, we elected to use temperature tuning, since strong shielding effects that are due to charge migration have been observed when static electric fields were applied to the MOTIRR.

For operation near $\Delta k = 0$, the variation of the wave-vector mismatch with temperature is given by

$$\delta(\Delta k L_{rt}) = \left.\frac{\partial \Delta k}{\partial T}\right|_{\Delta k=0} L_{rt}\delta T, \tag{6}$$

where $\partial\Delta k/\partial T = 7.5/(\text{cm K})$ at the phase-matching temperature of 107 °C for noncritical harmonic generation of 1064 nm in MgO:$LiNbO_3$. When the tuning parameters are adjusted, the optical-path length of the subharmonic is changed as well. The change in laser frequency ν_1 necessary to compensate for a change in resonator temperature is

$$\delta\nu_1 = -\nu_1\left(\frac{1}{n_o}\frac{\partial n_o}{\partial T} + \alpha\right)\delta T, \tag{7}$$

where α is the thermal-expansion coefficient. At 1.06 μm, $\delta\nu_1/\delta T \simeq -5.4$ GHz/k. When one combines Eqs. (6) and (7) the laser-frequency change required for tuning from one double resonance to the next is

$$\left|\frac{\Delta\nu_1}{\nu_{\text{FSR}}}\right| = \frac{2\pi n_o}{\lambda_0}\left(\frac{1}{n_o}\frac{\partial n_o}{\partial T} + \alpha\right)\left(\frac{\partial\Delta k}{\partial T}\right)^{-1}, \tag{8}$$

where ν_{FSR} denotes the free spectral range of the resonator. Here $|\Delta\nu_1| = 4.5$ GHz cm/L_{rt}, and FSR denotes free spectral ranges.

B. Internal Powers in Doubly Resonant Second-Harmonic Generation

Expressions for circulating subharmonic and harmonic powers as functions of the input power have been given by a number of authors.[8,12,15] A detailed derivation is available.[6]

Consider a ring cavity with subharmonic power P_{in} incident upon the (here FTIR) mirror N. Under double-resonance conditions, the intracavity subharmonic power P_1 and the harmonic power P_2 are[22]

$$P_1 = \frac{1 - [r_1^{(N)}]^2}{[r_1^{(N)}]^2}\frac{(r_1^{\text{conv}} r_1^{\text{tot}})^2}{(1 - r_1^{\text{conv}} r_1^{\text{tot}})^2}P_{\text{in}},$$

$$P_2 = \gamma_{\text{SHG}} L_{rt} G\left(\frac{r_2^{\text{tot}}}{1 - r_2^{\text{tot}}}\right)^2 P_1^2. \tag{9}$$

Here r denotes various amplitude reflection coefficients: $r_1^{(N)}$ is the input mirror reflection coefficient; r_i^{tot} are the round-trip reflection coefficients resulting from cavity losses (power loss coefficients a_i) and output couplings, or imperfect reflectivities of the mirrors [reflection coefficients $r_i^{(j)}$]:

$$r_i^{\text{tot}} = \exp(-a_i L_{rt}/2)\prod_{j=1}^{N} r_i^{(j)}. \tag{10}$$

The effective reflection coefficient r_1^{conv} describes the amplitude losses experienced by the subharmonic wave because of conversion losses:

$$r_1^{\text{conv}} = 1 - \gamma_{\text{SHG}} L_{rt} G\frac{r_2^{\text{tot}}}{1 - r_2^{\text{tot}}}P_1. \tag{11}$$

The product $\gamma_{\text{SHG}} L_{rt} G P_1$ is the single-pass conversion efficiency, with the focusing factor G defined below in Eq. (17), and

$$\gamma_{\text{SHG}} = \frac{2}{\pi}\frac{\omega_1^3 d_{\text{eff}}^2}{n^2 c^4 \epsilon_0}. \tag{12}$$

For $LiNbO_3$ and a subharmonic wavelength of 1.06 μm, $d_{\text{eff}} = 4.7$ pm/V,[23] and $\gamma_{\text{SHG}} = 0.22/\text{Wm}$. To make the connection to SHG in which only the subharmonic wave is resonated,[24] one must replace the enhancement term $r_2^{\text{tot}}/(1 - r_2^{\text{tot}})$ with unity in Eqs. (9) and with 1/2 in Eq. (11).

In the present study the following limiting cases are satisfied: small conversion losses, $1 - r_1^{\text{conv}} \ll 1$; small subharmonic input–output coupling, $1 - r_1^{(N)} \ll 1$; and small linear losses, $1 - r_i^{\text{tot}} \ll 1$. One can then approximate Eqs. (9) as

$$\left(1 + \frac{\gamma_{\text{SHG}} L_{rt} G\mathcal{F}_1\mathcal{F}_2}{\pi^2}P_1\right)(P_1)^{1/2} = \frac{\mathcal{F}_1}{\pi}(T_1 P_{\text{in}})^{1/2},$$

$$P_2 = \frac{\gamma_{\text{SHG}} L_{rt} G\mathcal{F}_2^2}{\pi^2}P_1^2. \tag{13}$$

We defined the power transmission coefficient T_1 for the subharmonic and the finesses as

$$T_1 = 1 - [r_1^{(N)}]^2, \qquad \mathcal{F}_i = \frac{\pi(r_i^{\text{tot}})^{1/2}}{1 - r_i^{\text{tot}}}, \tag{14}$$

respectively. In a MOTIRR the input mirror transmission $T_1 = T_1(x)$ and finesse $\mathcal{F}_1 = \mathcal{F}_1(x)$ are set by the distance x between the coupling prism and the resonator. The explicit dependencies of T and $\mathcal{F}$ on x are given in Ref. 6. Here it suffices to establish the relation between the subharmonic finesse and the input mirror transmission coefficient by defining the naked (large-gap) finesse $\mathcal{F}_1(x \to \infty) = \mathcal{F}_1[r_1^{(N)} = 1]$, whereby

$$T_1(x) = 2\pi\left[\frac{1}{\mathcal{F}_1(x)} - \frac{1}{\mathcal{F}_1(\infty)}\right]. \tag{15}$$

Returning to Eqs. (13) for the circulating powers, we note that the second term in parentheses represents the effect of conversion loss, which causes the circulating subharmonic power to change from a linear dependence on the input power to a slower $P_1 \propto P_{\text{in}}^{1/3}$ dependence (for constant T_1). The crossover point, when conversion losses start to dominate linear losses, occurs when the circulating subharmonic power reaches the value

$$P_1^* = \frac{\pi^2}{\gamma_{\text{SHG}} L_{rt} G\mathcal{F}_1\mathcal{F}_2}. \tag{16}$$

This value is also the threshold for DR near-degenerate parametric oscillation [$P_2(P_1^*) = P_2^{\text{th}}$; see Eq. (20) below].

C. Focusing Factor

In a MOTIRR cut as shown in Fig. 1, harmonic generation occurs on each of the ring legs. When the harmonic wave

generated on a leg propagates to the next leg, it will generally not be in phase with the harmonic wave generated there, since the TIR phase jump $\exp(i\gamma_s)$ experienced by the harmonic electric field is generally not equal to the phase jump $\exp(2i\gamma_p)$ of the square of the subharmonic electric field, which is the driving force for SHG. For example, in $LiNbO_3$ and 45° incidence, the relative phase jump is $\gamma_2 - 2\gamma_1 = 226°$. The individual harmonic waves generated on each leg will thus interfere, resulting in the focusing factor[6]

$$G = \left| \sum_{i=1}^{N} \left[\frac{l^{(i)}}{L_{rt}} \right]^{1/2} g[l^{(i)}, z_0^{(i)}, \Delta k] \prod_{j=1}^{i-1} \exp\{i[2\gamma_1^{(j)} - \gamma_2^{(j)}]\} \right|^2 . \tag{17}$$

The individual leg lengths are denoted by $l^{(i)}$, and g indicates the respective focusing factors. The latter are given, with the resonator's astigmatism taken into account, by

$$g(l, z_0, \Delta k) = \left(\frac{z_r}{2l} \right)^{1/2} \int_{z_0/z_r}^{(z_0+l)/z_r} \frac{\exp(-i\Delta k z_r \tau) d\tau}{[(1 + i\tau/\alpha)(1 + i\tau\alpha)]^{1/2}} . \tag{18}$$

Here z_0 is the distance from the beginning of the leg to the mode's waist location at $z = 0$. The beam propagates in the $+z$ direction (see Fig. 1). In the absence of astigmatism ($\alpha = 1$), $|g|^2$ reduces to the Boyd–Kleinman focusing factor h.[25] The focusing factor G was numerically calculated in Ref. 6. Interference effects in a standing-wave cavity were studied in Ref. 26.

3. OPTICAL PARAMETRIC OSCILLATION

A. Threshold for Oscillation

As the subharmonic input power is increased, the circulating harmonic power attains substantial levels, exceeding the input power by more than an order of magnitude for input powers >1 mW in this study. The question whether the stationary DR state will undergo any qualitative changes as the input power continues to grow arises. It was predicted[8] that a Hopf bifurcation to a time-dependent state occurs above an internal threshold power:

$$P_2^{sp} = \frac{\pi^2}{\gamma_{SHG} L_{rt} G \mathcal{F}_2^2} \left(1 + \frac{\mathcal{F}_2}{\mathcal{F}_1} \right)^2 . \tag{19}$$

The intracavity fields exhibit regular periodic pulsations at powers that exceed, but that are close to, this threshold.

The circulating harmonic can also act as a pump for internal parametric oscillation with nondegenerate signal and idler modes resonant with the cavity. The simultaneous occurrence of DR SHG and DR parametric oscillation may be called quadruply resonant parametric oscillation (QRO). A lower limit for the threshold is given by the expression for the degenerate DRO[25]:

$$P_2^{th} = \frac{\pi^2}{\gamma_{SHG} L_{rt} G \mathcal{F}_1^2} . \tag{20}$$

Note that the parametric gain is equal to the gain for SHG in type-I noncritical phase matching. Comparing Eqs. (19) and (20), we conclude that the parametric oscillation threshold is always lower than the self-pulsing threshold, regardless of the relative values of the finesses. Equation (20) for the DRO threshold assumes that signal and idler are perfectly resonant with cavity-mode frequencies. If such frequencies exist, DR SHG will preferentially lead to DRO rather than to self-pulsing. Self-pulsing is possible, however, if one chooses operating conditions (crystal temperature, electric field) such that all possible signal and idler pairs are sufficiently detuned to raise their oscillation thresholds above the self-pulsing threshold.

Inserting Eq. (20) into Eqs. (13) yields the corresponding input threshold power:

$$P_{in}^{th} = \frac{4\pi^4}{\gamma_{SHG} L_{rt} G \mathcal{F}_1^3 \mathcal{F}_2 T_1} . \tag{21}$$

In a MOTIRR this power still depends on the gap x, which controls the frustration of TIR, so that $\mathcal{F}_1 = \mathcal{F}_1(x)$ and $T_1 = T_1(x)$. Minimizing P_{in}^{th} with respect to x and using Eq. (15), we find that the minimum threshold occurs when the resonator is slightly undercoupled off double resonance, at $T_1(x_{opt}) = \pi/\mathcal{F}_1(\infty)$:

$$P_{in}^{th}|_{min} = \frac{27}{2} \frac{\pi^3}{\gamma_{SHG} L_{rt} G \mathcal{F}_1(\infty)^2 \mathcal{F}_2(\infty)} , \quad \text{(QRO)} . \tag{22}$$

Since the outcoupling of the harmonic at $x = x_{opt}$ is much smaller than the internal harmonic losses for the present MOTIRR's, we used $\mathcal{F}_2(x) \simeq \mathcal{F}_2(\infty)$ in proceeding from Eq. (21) to Eq. (22). Experimentally, one can set T_1 by measuring the subharmonic power P_r reflected from the MOTIRR off double resonance. We define the SR coupling coefficient c_1 for resonance of only the subharmonic:

$$c_1(x) = 1 - \left. \frac{P_r}{P_{in}} \right|_{SR} = \frac{2}{\pi} \frac{[\mathcal{F}_1(x)]^2}{\mathcal{F}_1(\infty)} T_1(x) . \tag{23}$$

At x_{opt} the resonator is slightly undercoupled off double resonance, with $c_1(x_{opt}) = 8/g$. In practice it is simpler to impedance match the MOTIRR when it is detuned from double resonance, $c_1 = 1$. In this case $T_1 = 2\pi/\mathcal{F}_1(\infty)$, $\mathcal{F}_1(x) = \mathcal{F}_1(\infty)/2$, and the numerical factor in Eq. (22) is increased to 16.

Parametric oscillation in a QRO can occur only if the resonator is undercoupled at double resonance. In particular, the oscillation threshold cannot be achieved if the input coupling for the subharmonic is chosen to give maximum circulating harmonic power. P_2 is maximized at impedance match on double resonance, [$c_{DR} = 1$ in Eq. (39) below], which requires an input mirror transmissivity

$$T_1^{opt} = \frac{\pi}{\mathcal{F}_1(\infty)} \left(1 + \left\{ 1 + \frac{2}{\pi^3} \gamma_{SHG} L_{rt} G [\mathcal{F}_1(\infty)]^2 \mathcal{F}_2 P_{in} \right\}^{1/2} \right) , \tag{24}$$

which yields a circulating power $P_1^{opt} = P_{in} T_1^{opt}$. We assumed in the derivation that the finesse and the output coupling of the harmonic wave are independent of T_1. Comparing P_1^{opt} with the threshold [Eq. (16)], we find that

$$\frac{P_1^{opt}}{P_1^*(T_1^{opt})} = \frac{T_1^{opt} - 2\pi/\mathcal{F}_1(\infty)}{T_1^{opt} + 2\pi/\mathcal{F}_1(\infty)} < 1 . \tag{25}$$

It is interesting to compare the threshold input power of a QRO at the subharmonic frequency with that of a TRO

at the harmonic frequency. Consider Eqs. (13) together with Eq. (15), which describe, in the absence of conversion, $\gamma_{SHG} = 0$, the internal enhancement of a cold cavity. The maximum enhancement of the pump is seen to occur for impedance match

$$T_2^{opt} = \frac{\pi}{\mathcal{F}_2(\infty)}, \qquad P_2^{max} = \frac{\mathcal{F}_2(\infty)}{2\pi} P_{2,in}. \tag{26}$$

Using threshold Eq. (20) and assuming that the output coupling of the signal and the idler is chosen for maximum external power, $\mathcal{F}_1(x) = \mathcal{F}_1(\infty)/2$, we obtain

$$P_{2,in}^{th} = \frac{8\pi^3}{\gamma_{SHG} L_{rt} G \mathcal{F}_1(\infty)^2 \mathcal{F}_2(\infty)}, \qquad \text{(TRO)}. \tag{27}$$

This result is approximately one half of the minimum threshold of a QRO, which is given by Eq. (22).

Note that, for operation of the QRO off degeneracy, the parametric gain and the SHG gain differ and the external threshold increases because of the decrease in the SHG gain.

Once the internal harmonic power exceeds the oscillation threshold, one must modify Eqs. (13) for the DR SHG intracavity powers to take into account the losses resulting from generation of signal and idler waves. This can be accomplished by a straightforward analysis of the steady-state solution of the four coupled amplitude equations that is similar to the analysis of the TRO.[17]

B. Output Spectrum

The tuning behavior of the output wavelengths of an OPO as a function of tuning parameters such as pump frequency and resonator temperature was recently investigated in detail for type-I[21] and for type-II[27] phase matching. Here we discuss tuning properties associated with interference effects, operation below the phase-matching temperature, and quadruple-resonance effects.

An OPO will preferentially oscillate at that signal–idler pair whose threshold is minimum. The threshold depends on, among other things, the detunings of signal and idler frequencies from their respective cavity resonances and on the parametric gain, all of which are functions of resonator temperature and signal (or idler) wavelength. One can explain the coarse-tuning properties of an OPO on an angstrom scale by considering both the wavelength–temperature relation (cluster curve) that describes average zero signal–idler detuning and photon energy conservation, and the wavelength–temperature values that yield large parametric gain. In addition, a fine structure, determined by the modal spacing of the resonator, governs the actual signal–idler mode hops.

Consider first a DRO. The operating conditions are determined by three equations, namely, two resonance conditions for signal and idler frequencies as given by Eq. (1) and the energy conservation relation. Given an arbitrary pump (harmonic) frequency $\omega_2 = \omega_s + \omega_i$ and signal and idler mode numbers $M_{s,i}$, the three equations permit a unique solution (T, ω_s, ω_i). One can understand this solution as arising from the intersection of a so-called cluster curve $\omega_s^{CL}(T)$ associated with the value of $M_i + M_s$ and the signal resonance curve $\omega_s(T)$ associated with the value of M_s. In this picture a DRO differs from a TRO in that the pump frequency is arbitrary for the former but is, through the pump-frequency resonance condition, a function of temperature for the latter.

To find the cluster curves, we consider expansions of the resonance equations for signal and idler waves for small deviations of their frequencies and of the resonator temperature from some arbitrarily chosen reference point ω_0, T_0. Dispersion, thermo-optic effect, and thermal expansion α result in resonator index and length changes, which are given by

$$n_o(T, \omega) \simeq n_o(T_0, \omega_0) + \frac{\partial n_o}{\partial T}\Delta T + \frac{\partial n_o}{\partial \omega}\Delta\omega + \frac{1}{2}\frac{\partial^2 n_o}{\partial \omega^2}\Delta\omega^2, \tag{28}$$

$$L_{rt}(T) \simeq L_{rt}(T_0)[1 + \alpha(T_0)\Delta T], \tag{29}$$

with the deviations $\Delta\omega_{s,i} = \omega_{s,i} - \omega_0$ and $\Delta T = T - T_0$. From Eq. (1) we obtain

$$A\Delta T + 2B\Delta\omega_{s,i} + C\Delta\omega_{s,i}^2 = M - m_0 - \frac{\Phi}{2\pi}, \tag{30}$$

where $m_0 = \omega_0/\omega_{FSR}$, the MOTIRR-cavity free spectral range is $\omega_{FSR} = 2\pi c/nL_{rt}$, Φ is the sum of TIR and Guoy phase shifts, and the coefficients are defined by

$$A = m_0\left(\frac{1}{n_o}\frac{\partial n_o}{\partial T} + \alpha\right), \qquad B = \frac{1}{2\omega_{FSR}}\left(\frac{\omega_0}{n_o}\frac{\partial n_o}{\partial \omega} + 1\right),$$
$$C = \frac{1}{n_o \omega_{FSR}}\left(\frac{\omega_0}{2}\frac{\partial^2 n_o}{\partial \omega^2} + \frac{\partial n_o}{\partial \omega}\right). \tag{31}$$

For $LiNbO_3$ (Ref. 21) and $\lambda_0 = 1064$ nm, $T_0 = 107\,^\circ$C, $L_{rt} = 3.2$ cm (square MOTIRR), we find that $A = 1.3\ K^{-1}$ is dominated by the expansion coefficient $\alpha(T_0)$, $B = 2.0 \times 10^{-11}$ s/rad is dominated by the inverse resonator free spectral range, and $C = 7.2 \times 10^{-28}$ (s/rad)^2 is dominated by the first-order frequency derivative of the index.

Summing the signal and idler resonance frequency equations [Eq. (30) for signal plus Eq. (30) for idler] and using the photon energy conservation relation, we obtain the cluster equation

$$A\Delta T + C(\Delta\omega_s^{CL})^2 + (B - C\Delta\omega_s^{CL})\Delta\omega_2 + C\Delta\omega_2^2 = \frac{M_s + M_i}{2} - m_0 - \frac{\Phi_s + \Phi_i}{4\pi}. \tag{32}$$

Here we have defined $\Delta\omega_2 = \omega_2 - 2\omega_0$. The intersections of the cluster curves $\Delta\omega_s^{CL}(\Delta T)$ defined by this equation, along with the resonance equation (30) for $\Delta\omega_s$, define the operating frequencies for a DRO or a TRO. Equation (32) was studied by Eckardt *et al.*[21] for DRO's. In their study the harmonic wave is provided by a separately frequency-doubled laser with fixed frequency, $\Delta\omega_2 = 0$, and the cluster curves are parabolas that open toward decreasing temperature.

In a TRO an additional resonance condition is imposed. TRO's discussed in the literature[17,19] are those in which the pump frequency coincides with a cavity mode.

For the present discussion of the QRO it is convenient to take the subharmonic (laser) resonance condition as the third resonance condition and to impose the resonance condition of the harmonic (OPO pump) later. Since the subharmonic is an ordinary wave, the resonance condition

for the laser frequency when the laser is frequency locked to the MOTIRR is the same as Eq. (30) for the signal and the idler. Defining the previously introduced ω_0 as the resonant laser frequency ω_1 when $T = T_0$, we obtain

$$2B\Delta\omega_1 = M_1 - m_0 - \frac{\Phi_1}{2\pi} - A\Delta T. \tag{33}$$

Higher-order terms have been neglected, since in practice the tuning range $\Delta\omega_1$ of the laser is small. When the MOTIRR temperature is changed so much that a particular MOTIRR mode is forced outside the laser's tuning range, the laser frequency must be reset to coincide with a neighboring mode, $M_1 \rightarrow M_1 \pm 1$.

Combining Eqs. (32) and (33) and using $\omega_2 = 2\omega_1$, $\Delta\omega_2 = 2\Delta\omega_1$ yield

$$C(\Delta\omega_s^{\mathrm{CL}})^2 = \frac{M_s + M_i}{2} - M_1 + \frac{\Phi_1}{2\pi} - \frac{\Phi_s + \Phi_i}{4\pi}. \tag{34}$$

The cluster curves for a QRO (but not a TRO) are temperature independent because the tuning coefficients of the signal, idler, and subharmonic (laser) frequency are equal near degeneracy. The first cluster curve, $\Delta\omega_s^{\mathrm{CL}} \simeq 0$, and the second cluster curve, given by a change of unity in $M_s + M_i$, are spaced by a signal-wavelength difference $\delta(\Delta\omega_s) \simeq 1/\sqrt{2C}$, or 17 nm here.

Whereas both triple resonance and double resonance can be satisfied for a set of temperatures and signal-frequency values (T, ω_s) labeled by M_s, M_i, the fourth condition in quadruple resonance overdetermines these, and in general no solution is possible. To permit near-quadruple resonance, we must permit slight detunings in the signal, idler, and harmonic waves, which can be incorporated into Φ_s, Φ_i, and Φ_2. Signal and idler detunings lead to an increase in oscillation threshold, and harmonic detuning leads to a reduction in harmonic power. As long as the subharmonic power is sufficiently strong, the harmonic power will be large enough for oscillation to occur.

A further factor in permitting quadruple resonance is given by the freedom in the choice of signal and idler transverse modes. A laser locked to a TEM_{00} subharmonic resonator mode generates only a TEM_{00} harmonic mode. However, a TEM_{00} harmonic mode can couple to higher-order transverse TEM_{nm} signal and idler modes u_{nm}, since the modal overlap $\int (u_{2,00})^* u_{s,nm} u_{i,nm} \mathrm{d}x\mathrm{d}y$ is nonzero for $n, m \neq 0$. We verified the existence of this coupling experimentally, after we misaligned the MOTIRR, by the inverse process of generating the TEM_{00} harmonic mode from a TEM_{01} subharmonic mode to which the laser was frequency locked.

Finally, on double resonance, the absorption of the circulating waves leads to local heating effects that require modification of the above simple resonance equations based on a homogeneous resonator temperature. Additional degrees of freedom in the temperature distribution can permit quadruple resonance.

4. EXPERIMENTAL RESULTS

A. Experimental Setup

Two MOTIRR's were fabricated from a 5% MgO:$LiNbO_3$ crystal (Fig. 1). The square MOTIRR has dimensions of 11 mm × 11 mm × 2 mm, yielding a ring length of L_{rt} = 3.2 cm, with three flat faces and one curved (R = 25 mm) face. The second device, of the same thickness, has two flat faces and one curved (R = 9 mm) face, yielding an equilateral triangular ring with L_{rt} = 1 cm. The c axis of the crystal is perpendicular to the ring plane in both devices. Gold coatings were deposited onto the top and bottom faces of the MOTIRR's. During alignment of the resonator a high-voltage ramp can be applied for electro-optic tuning over a free spectral range.

The experimental setup is shown in Fig. 2. The subharmonic laser is a 1.06-μm Nd:YAG laser-diode-pumped nonplanar ring oscillator. The laser beam is expanded and collimated, and two cylindrical lenses are used to match the laser beam to the resonator TEM_{00} modes. Their waists are given by Eqs. (3); for the square MOTIRR w_x = 24 μm and w_y = 51 μm; for the triangular MOTIRR w_x = 24 μm and w_y = 28 μm. We determined the focal lengths of the lenses by calculations that used the $ABCD$-matrix formalism, in which we assumed that the interface of prism, air gap, and MOTIRR acts as a spherical interface between two dielectrics, $LiNbO_3$ and the prism material. We achieved as much as 95% mode matching.

The MOTIRR and the prism assembly are mounted on a base plate, which is itself mounted on a compact stage that permits fine control of all six degrees of freedom of the MOTIRR setup relative to the laser beam. The alignment is greatly facilitated by a visible alignment laser diode mounted on the base plate and used for both orienting the prism with respect to the MOTIRR and producing a scatter spot on the prism coupling face at the input point. The setup is displaced until the laser beam and the scatter spot overlap.

The SF-6 coupling prism is mounted on a translation stage. Coarse control of gap distance is obtained by a micrometer screw, and fine control by a piezoelectric transducer with 20-μm throw. We monitor the gap distance by observing Newton's fringes produced by the alignment laser. The intensity of the central fringe can be employed as an error signal for active gap stabilization by use of a feedback loop, but this was not necessary in the present experiment.

Both the MOTIRR and the prism are heated. The MOTIRR oven consists of two copper blocks between

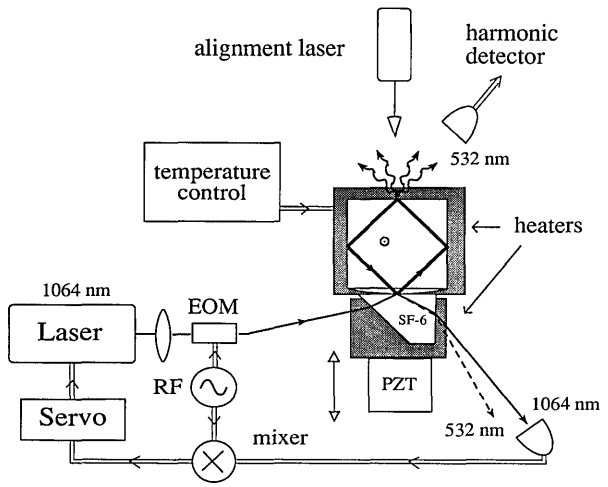

Fig. 2. Experimental setup for DR SHG and QRO in a MgO:$LiNbO_3$ MOTIRR. EOM, electro-optic modulator; PZT, piezoelectric transducer; RF, 12-MHz quartz oscillator.

which the resonator is placed. The copper blocks also serve as contact electrodes for electro-optic tuning. The temperature sensor for the MOTIRR oven is inserted into the lower copper block. The relative heater powers are optimized to yield the narrowest possible phase-matching curve for the single-pass SHG of a subharmonic wave traversing the MOTIRR normal to the two opposing flat faces. The coupling prism is heated by an independent heater, driven by a constant current source, without active temperature control. Good passive isolation from air currents and partial isolation from acoustic noise is provided by an acrylic plastic housing enclosing MOTIRR, ovens, prism, prism holder, and prism translation stage. After optimization of oven feedback control parameters, good frequency stability of the MOTIRR is obtained, with drifts of <10 MHz/min.

Frequency lock of the laser to the MOTIRR is accomplished by use of the frequency-modulation technique,[28] which yields an error signal that is fed back to a slow and a fast frequency-control actuator on the laser. The laser beam is phase modulated at 12 MHz by an electro-optic modulator, and the beam reflected from the resonator is detected and amplified by a low-noise photodetector. The ac signal and an appropriately phase-shifted local oscillator are fed into a mixer. The baseband output of the mixer is amplified by a variable-gain servo amplifier with a −3-dB frequency of 10 Hz and is fed into the fast laser frequency actuator, a piezoelectric transducer attached to the laser resonator. The error signal is also input into an integrator whose output controls the temperature of the laser crystal.

The subharmonic output of the MOTIRR (reflected input power and signal and idler waves) is analyzed spectrally with a Fabry–Perot cavity and with a grating spectrometer and temporally with a fast photodetector.

A detector insensitive to infrared light is placed close to the MOTIRR to detect a fraction of the light scattered from the circulating harmonic wave.

B. Characterization of the Monolithic Total-Internal-Reflection Resonator

Resonator Losses and Tuning Coefficients

We determined the parameters used in Eqs. (13) experimentally. We measured the finesse at the subharmonic frequency in the usual manner by phase modulating the laser beam and performing a frequency scan of the laser across the MOTIRR resonance while recording the power reflected from the cavity. In the spectrum the comparison of FWHM of the carrier resonance and the spacing of the phase-modulation sidebands yields the linewidth. In the limit of a large gap, when the finesse is determined by the resonator losses only, $\mathcal{F}_1(\infty) = 1.5 \times 10^2$ for the p-polarized (ordinary) wave, implying round-trip resonator loss of 0.4% at 1.06 μm for the $L_{rt} = 3.2$-cm-long ring. The finesse of the extraordinary wave was higher: $\mathcal{F}_1(\infty) = 2.1 \times 10^2$. For the MOTIRR with the 1-cm round-trip ring length, the o finesse is 3.0×10^2, implying a 0.2% loss. The absorption loss of $LiNbO_3$ of the same origin was measured by laser absorption calorimetry to be 0.14%/cm,[29] which accounts for most of the losses. Below we discuss only the square MOTIRR.

In the absence of a laser source at the harmonic frequency, one can indirectly determine the finesse $\mathcal{F}_2$ by measuring the variation of intracavity harmonic power while the laser is locked to the MOTIRR and the temperature is slowly ramped through a double resonance.[6,11] Such a scan is shown in Fig. 3. The circulating harmonic power as a function of detuning from double resonance can be written as an Airy function:

$$P_2 = \frac{\gamma_{SHG}}{4\pi^2} L_{rt} G \frac{r_2^{tot} \mathcal{F}_2^2}{1 + (2\mathcal{F}_2/\pi)^2 \sin^2(\arg r_2^{tot}/2)} P_1^2. \quad (35)$$

Here the phase of the round-trip reflection coefficient, $\arg r_2^{tot}$, is given by the left-hand side of Eq. (2). When the subharmonic is frequency locked to the MOTIRR Eq. (1) is satisfied, and Eq. (35) reduces to

$$P_2(T) \propto \frac{P_1^2}{1 + (2\mathcal{F}_2/\pi)^2 \sin^2\{[\Delta k L_{rt}(T) + \Phi]/2\}}, \quad (36)$$

where Φ contains essentially temperature-independent Guoy and TIR phase shifts. In the very-low-power ($P_{in} \sim \mu$W) limit, the circulating subharmonic power P_1 in relation (36) is approximately independent of the resonance of the harmonic. Thus the harmonic power has a Lorentzian line shape as a function of temperature (the focusing factor varies slowly with temperature), with a FWHM in temperature given by

$$\Delta T_{FWHM} = \frac{2\pi}{\mathcal{F}_2} \left(\frac{\partial \Delta k L_{rt}}{\partial T} \right)^{-1}. \quad (37)$$

The finesse of the double resonance in temperature space is thus identical to the finesse in frequency space: $\mathcal{F}_2 = \Delta T_{DR}/\Delta T_{FWHM}$. In this way we determine a finesse of ~200 (3% loss) at 532 nm for the square MOTIRR.

We measured the tuning coefficients derived in Subsection 2.A by applying a known temperature change to the MOTIRR and by measuring, with a 300-MHz Fabry–Perot cavity, the required laser-frequency change that compensates for the mode-frequency shift. The measured temperature-tuning coefficient is $\delta\nu_1/\delta T = 5.8$ GHz/K, in good agreement with the predicted value. It is also possible to measure a particular combination of tuning parameters by measuring the frequency interval over which the locked laser must be tuned during a temperature scan over subsequent double resonances. The predicted value [Eq. (8)] for $\Delta\nu_1/\nu_{FSR}$ is 0.34; the measured value for the 1-cm ring-length MOTIRR is 4.1/12.7 GHz = 0.32, in good agreement.

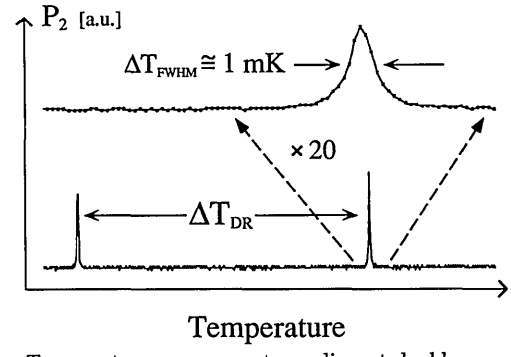

Fig. 3. Temperature scan over two adjacent double resonances. At low subharmonic powers the ratio of splitting to FWHM yields the harmonic finesse.

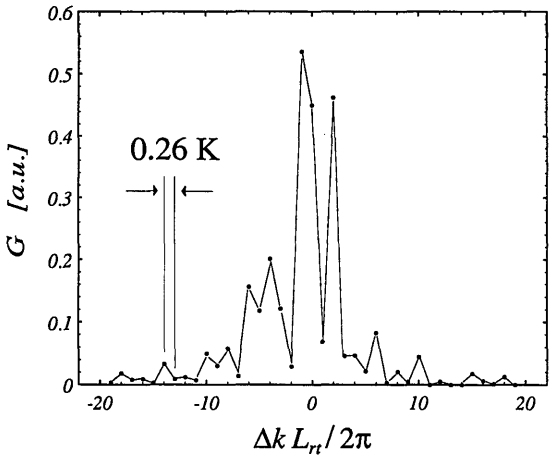

Fig. 4. MOTIRR phase-matching curve. The variations in focusing factor G are due, in part, to the interference effects between the harmonic waves generated on the four legs.

Conversion Coefficient

Before we measured the conversion coefficient $\gamma_{SHG} G L_{rt}$, we varied the temperature distribution within the MOTIRR by changing the current to the coupling prism heater until we observed maximum harmonic intracavity power at one of the double resonances. This procedure does not guarantee a homogeneous temperature distribution within the resonator; therefore a detailed comparison with the theoretical prediction of Eq. (17) was not possible.

Figure 4 shows the phase-matching curve for DR SHG, consisting of the relative values of intracavity harmonic power $P_2(\Delta k L_{rt})$ at the double-resonance–wave-vector mismatch values defined by Eq. (5). The measurement is performed at very low power levels so that the conversion loss is small compared with the loss of the cold cavity. The harmonic detector signal is then proportional to the focusing factor.

In principle, one can derive the absolute value of single-pass conversion efficiency $\gamma_{SHG} G$ of the strongest double resonance by measuring the harmonic power P_2^{ext} extracted from the MOTIRR through the coupling prism. When the coupling coefficient of the harmonic wave is defined by analogy with Eq. (23), the gap dependence of the harmonic power is, from Eq. (13),

$$P_2^{ext}(x) = T_2(x) P_2(x) = \frac{\gamma_{SHG} L_{rt} G}{2\pi} c_2(x) P_1^2(x). \qquad (38)$$

Because of the difference in wavelength and loss, the harmonic coupling $c_2(x)$ varies exponentially at gap distances for which the subharmonic coupling is close to impedance match.[3] Since a determination of c_2 or of the harmonic transmission coefficient is difficult, the conversion efficiency is more accurately measured indirectly rather than through the extracted harmonic power.

The indirect measurement technique consists of measuring the increase in reflected subharmonic power P_r during the transition from SR SHG to DR SHG. The coupling of the subharmonic on double resonance is a function of all internal resonator losses, including losses that are due to conversion to the harmonic[6]:

$$c_{DR} = 1 - \left.\frac{P_r}{P_{in}}\right|_{DR} = \frac{1 - |r_1^{(N)}|^2}{(1 - r_1^{conv} r_1^{tot})^2}\left[1 - \frac{(r_1^{conv} r_1^{tot})^2}{|r_1^{(N)}|^2}\right]. \qquad (39)$$

Off double resonance the conversion losses $1 - r_1^{conv}$ are essentially zero, and this expression reduces to Eq. (23). Figure 5(a) schematically shows the effect of increased losses experienced by the subharmonic wave on double resonance. When one expresses c_{DR} in terms of the subharmonic circulating power by use of Eqs. (9), (15), and (16),

$$\frac{c_{DR}(x)}{c_1(x)} = \left[1 + \frac{\mathcal{F}_1(\infty)}{\mathcal{F}_1(x)} \frac{P_1}{P_1^*}\right]\left(1 + \frac{P_1}{P_1^*}\right)^{-2}, \qquad (40)$$

it can be seen that, if $\mathcal{F}_1(\infty)/\mathcal{F}_1(x) < 2$ (i.e., if the resonator is undercoupled or inpedance matched at single resonance), the DR coupling is reduced compared with single resonance. Also, for a given input power, the decrease in DR coupling is stronger for smaller SR coupling. Figure 5(b) shows the experimental temperature dependence of the intracavity harmonic power and the concomitant increase in reflected subharmonic power at double resonance. We performed a series of such scans, using a range of input powers. Figure 6 shows the experimental results for two gap settings together with a fit based on Eq. (40). The single fit parameter in Fig. 6 is the effectively phase-matched length $L_{rt} G$ ($\gamma_{SHG} = 0.22/\mathrm{Wm}$ is used). For both values of c_1 we found the effective lengths to be $L_{rt} G = 1.4$ cm within experimental accuracy. The data increasingly scatter at input powers greater than 1 mW because optical parametric oscillation occurs, and the resonance lines become distorted (see Fig. 8 below).

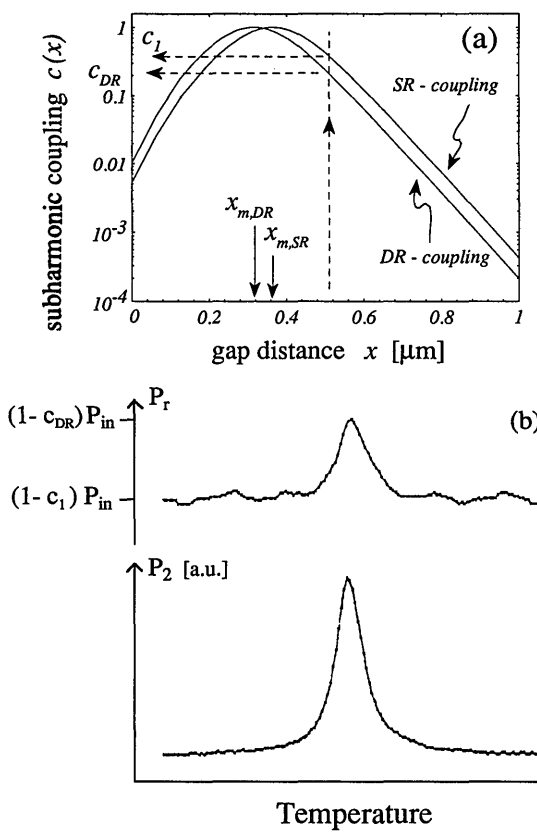

Fig. 5. Coupling reduction on double resonance. (a) The higher internal conversion losses effectively shift the coupling curve to smaller gaps; the coupling at fixed gap $x > x_{m,SR}$ is therefore reduced. (b) Reflected subharmonic power P_r and circulating harmonic power P_2 during temperature scan over double resonance.

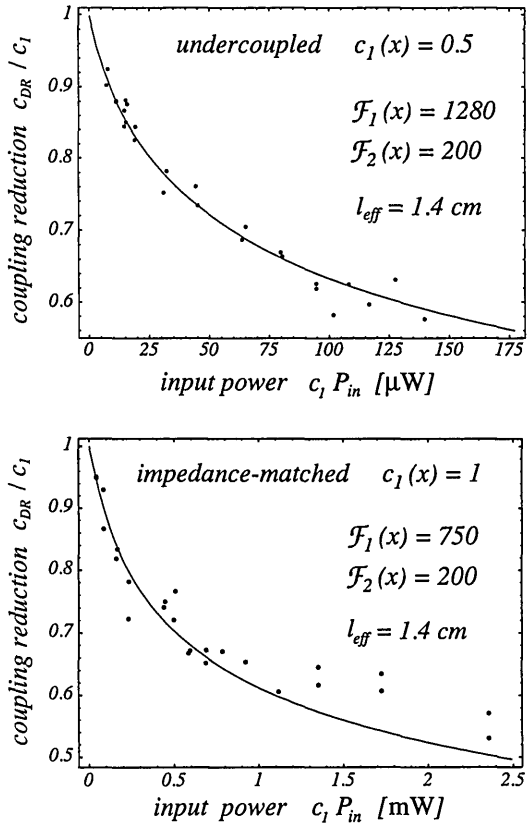

Fig. 6. Power dependence of coupling reduction for two values of single-resonance coupling. Circles, data; curves, theory, with $l_{\text{eff}} = L_{rt}G$ as the fit parameter. Plotting the coupling reduction versus the in-coupled power $c_1 P_{\text{in}}$ rather than versus P_{in} compensates for small deviations of the manually maintained SR coupling c_1 from its nominal value.

Knowledge of the conversion efficiency allows one to calibrate the measurement of harmonic power scattered into the external detector in order to calculate the internally circulating harmonic power. Figure 7 shows the intracavity harmonic power as a function of subharmonic input power.

C. Parametric Oscillation

One can calculate the thresholds for quadruply resonant parametric oscillation in the square MOTIRR by using Eqs. (13), (20), and (21). Under impedance match off double resonance [$c_1 = 1$, $\mathcal{F}_1 = \mathcal{F}_1(\infty)/2$], internal thresholds $P_1 = 21$ mW at 1.06 μm and $P_2 = 5.7$ mW at 532 nm and an external threshold $P_{\text{in}}{}^{\text{th}} = 0.36$ mW at 1.06 μm are predicted for the square MOTIRR. Experimentally, the OPO threshold occurred at an input power $P_{\text{in}}{}^{\text{th}} = 0.4$ mW, in good agreement with the above prediction. The onset of oscillation occurred with nondegenerate signal and idler modes and was observed with the grating spectrometer.

Figure 8 shows a typical temperature scan over a double resonance far above threshold. As the double resonance is approached, one observes a succession of different signal–idler mode pairs on the Fabry–Perot spectrum analyzer. These mode jumps can be jumps between longitudinal ($M_{i,s}$) and/or transverse modes. We did not perform signal–idler mode discrimination because of their spatial overlap with the laser beam reflected from the cavity. As verified by the grating spectrometer, the mode jumps usually did not lead to appreciable wavelength jumps, indicating that the signal–idler pairs occurred near the same Δk curve. We also observed simultaneous stable oscillation of two pairs. The absence of competition implies that the two pairs corresponded to different transverse resonator modes.

One can achieve stable operation with a single signal–idler mode pair by stopping the temperature scan at particular temperatures (Fig. 9). We observed as much as 15 min of continuous mode-hop-free operation under laser-frequency lock and MOTIRR temperature control.

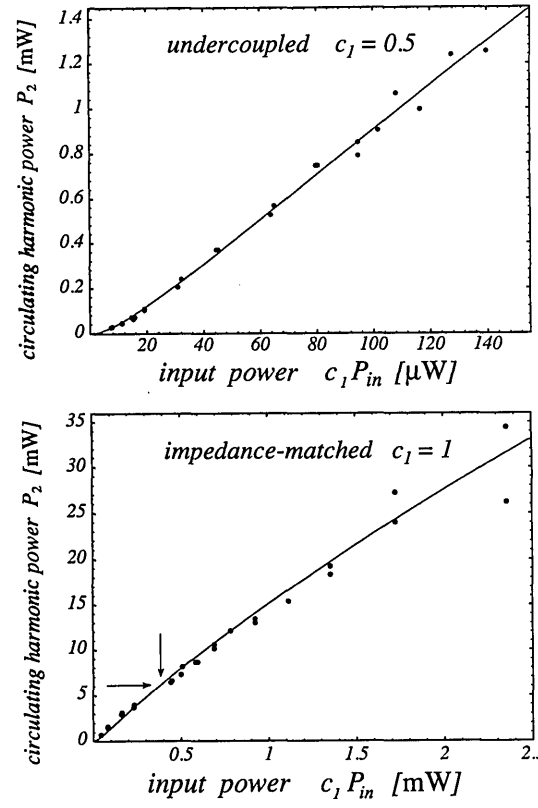

Fig. 7. Circulating harmonic power in DR SHG for two values of the subharmonic coupling. Curve, theory; circles, data scaled by a constant factor, since one can infer only the relative circulating powers from scattered powers. The arrows indicate the onset of parametric oscillation.

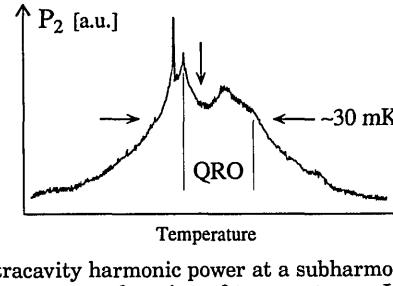

Fig. 8. Intracavity harmonic power at a subharmonic–harmonic double resonance as a function of temperature. Input power is several orders of magnitude larger than in Fig. 3, and thermal effects resulting from absorption of the circulating harmonic power cause the double resonance to widen significantly. Parametric oscillation occurs in the region between the lines, with a signal–idler mode jump at the arrow's position. Scan direction is from right to left.

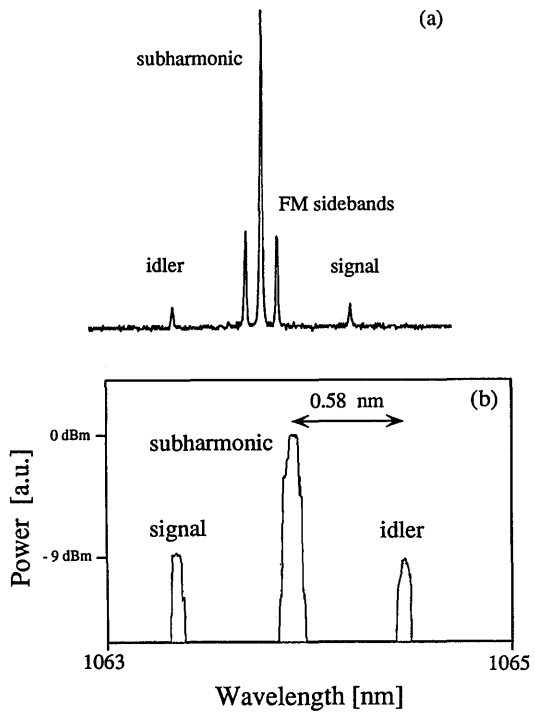

Fig. 9. Stable single-mode quadruply resonant parametric oscillation with small detuning of the harmonic from resonance. Spectral analysis of the infrared output from the resonator by (a) scanning the Fabry–Perot spectrum (300-MHz free spectral range). The phase-modulation sidebands required for frequency locking appear on either side of the subharmonic (laser). (b) Spectrum recorded by a grating spectrometer (resolution 0.1 nm). The subharmonic power at 1.06 μm is $P_{in} \simeq 2$ mW. The power in the signal and idler is ~0.3 mW each.

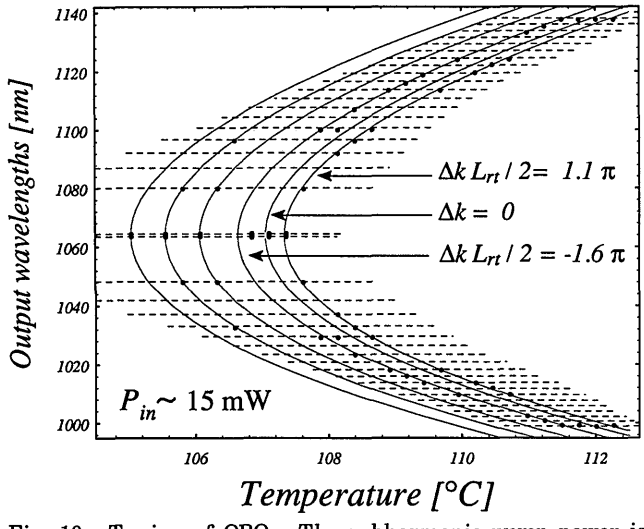

Fig. 10. Tuning of QRO. The subharmonic pump power is $P_{in} \simeq 15$ mW. The dashed lines represent the cluster curves calculated from Eq. (34). The curves represent loci of constant wave-vector mismatch $\Delta k L_{rt}$ calculated from Eq. (41). The circles represent the experimental wavelengths. The tuning fine structure governed by the resonance condition for the subharmonic is not shown.

A full tuning spectrum of the QRO is shown in Fig. 10. We did not measure the temperature values of the double resonances; we calculated their spacing with the index-of-refraction expression appropriate to $MgO:LiNbO_3$ (Ref. 21) and chose a temperature offset to center the $\Delta k L_{rt} = 0$ phase-matching curve with respect to the data above 107 °C. Treating the sum of phase shifts on the right-hand side of the cluster equation [Eq. (32)] as a free parameter, we obtain a good overall fit to the wavelength data by using the value $2\Phi_1 - \Phi_s - \Phi_i \simeq 0$, indicating that most of the data correspond to signal and idler modes identical to the harmonic, TEM_{00}, mode. Deviations from the fit can be explained by oscillation on higher-order transverse modes and deviations from the simple behavior of Eq. (34) when signal and idler are sufficiently far from degeneracy.

Oscillation occurs on the cluster curve where the wave-vector mismatch gives maximum parametric gain $\gamma_{SHG} L_{rt} G(\Delta k L_{rt})$. One can measure the parametric gain independently of any observation of parametric oscillation by measuring the conversion efficiency in SHG (Fig. 4). G is obtained easily only for discrete values of wave-vector mismatch, those corresponding to subharmonic–harmonic double resonances. Since the focusing factor exhibits local maxima at discrete values $\Delta k|_m$, the output wavelengths of an OPO tend to lie as close as possible to the curves $\Delta k(T, \lambda_s) = \Delta k|_m$. To find these curves it is useful to expand the wave-vector mismatch function near the degeneracy point $(T_d, \lambda_s = \lambda_i =: \lambda_d)$, where $\Delta k(T_d, \lambda_d) = 0$. Using the index-of-refraction expression for 5% $MgO:LiNbO_3$, we find that

$$\Delta k = [7.49(T - T_d)\,\mathrm{K}^{-1} - 8666(1 - \lambda_d/\lambda_s)^2]\ \mathrm{cm}^{-1}, \quad (41)$$

where $\lambda_d = 1064$ nm and $T_d = 107.05$ °C. Curves of constant $\Delta k L_{rt}$ are parabolas open toward increasing temperature, with apexes at $\lambda_s = \lambda_d$. According to Eqs. (34) and (41), at a fixed temperature the wave-vector mismatch $\Delta k L_{rt}$ changes by ~6.1 from one cluster curve to the next.

Returning to the QRO spectrum, we found that for temperatures above the phase-matching temperature (107 °C) most oscillation frequencies occur near two constant wave-vector-mismatch curves that are spaced apart by $\delta(\Delta k L_{rt}) \simeq 17$. This is a consequence of the interference taking place in the MOTIRR. The SHG conversion efficiency (Fig. 4) indeed reveals that $G(\Delta k L_{rt})$ exhibits a double-peaked structure with a spacing consistent with the above value of $\delta(\Delta k L_{rt})$. Off-degeneracy oscillation below the phase-matching temperature occurs because along the degeneracy line $(T, \lambda_s = \lambda_d)$ the focusing factor G varies as a function of temperature, exhibiting minima. This effect occurs for any type of resonator and does not require interference effects. However, the presence of interference effects determines the particular shape of the parametric-gain (here, the focusing factor) curve and the OPO tuning curve. In this case, for example, we can infer that off-degeneracy operation at 106.6 °C is due to the very small parametric gain at the value of $\Delta k L_{rt}$, corresponding to quasi-degenerate operation (the data point to the left of maximum in Fig. 4). For a similar reason oscillation did not occur (at the given subharmonic power) at the 105.3 °C double resonance.

5. CONCLUSION

In this study we have demonstrated what is, to our knowledge, the first quadruply resonant parametric oscillator. The external threshold at 1.06 μm (0.4 mW) is the lowest threshold demonstrated for optical parametric oscillators

to date. The internal threshold at 532 nm (6 mW) is the lowest value demonstrated in $LiNbO_3$. We obtained this result by using a MOTIRR that exhibited losses that were significantly lower than those of any previously described multiply resonant device (harmonic finesse ≈200, subharmonic finesse ≈750 at impedance match). The threshold is limited by the bulk losses of the MOTIRR, and one can further reduce it by reducing its size, as indicated by the lower losses exhibited by a 1-cm ring-length MOTIRR.

The QRO was operated with stable and single-frequency output. We tuned the output wavelengths between 1000 and 1140 nm, although a much wider tuning range could easily be achieved, thanks to the absence of narrow-band dielectric multilayer coatings. The QRO threshold will, however, rise because of the reduced harmonic generation efficiency. We explained the structure of the output spectrum below and above the degeneracy temperature with the help of the measured phase-matching (focusing-factor) curve.

A QRO is a useful device when the harmonic (pump) radiation is not available directly from a laser, since in this case a separate frequency-doubling device is required. A QRO requires significantly less power to reach threshold than does a doubling-stage–DRO combination. This is also the case for a doubling stage–TRO combination, unless the doubling stage's efficiency is greater than 50%.

The inherently low loss of MOTIRR's and the impedance matchability make nonlinear devices with high efficiency possible. Low oscillation thresholds can be exploited for cw frequency conversion of low-power single-frequency lasers, such as external-cavity diode lasers, or when low-nonlinearity materials are used. Particularly attractive is the possibility of extending OPO tunability far beyond that possible with resonators that employ multilayer mirrors by use of temperature-tuned noncritical phase matching or tunable pump sources. This also holds for SHG, where lithium triborate, with a tuning range from at least 0.95 to 1.65 μm[30] and low bulk loss,[19] is an excellent candidate material.

An extension of the MOTIRR design to biaxial crystals such as KTP is possible in conjunction with a recently developed highly symmetric resonator geometry.[31] A little-studied device, the cw SRO[32] can also be realized with MOTIRR's, and the ensuing loss reduction promises to reduce the threshold below 1 W for a $LiNbO_3$ SRO pumped at 532 nm.

MOTIRR's are also attractive for the study of dynamic instabilities. In the present study, we observed pulsation of the subharmonic wave reflected from the resonator on double resonance at high subharmonic power levels, with frequencies in the 12–16-MHz range and amplitude at ~40% of the dc level. This effect is now under study. One can analyze such effects theoretically by examining the stability of the steady-state solution of the four coupled amplitude equations in the presence of detuning, extending the treatment of the dynamics of the degenerate TRO[33] to the QRO.

The demonstration of self-pulsing in DR SHG in the absence of parametric oscillation is an important next step. The self-pulsing threshold depends strongly on the losses at the harmonic frequency as well as the input transmission of the subharmonic and could easily be minimized in a MOTIRR through gap control.

Another application that could benefit from optimizable input–output couplings in MOTIRR's is the generation of nonclassical radiation.[10]

Finally, a MOTIRR could also provide an alternative to calorimetry and integrating sphere measurements for the determination of total bulk losses of materials. One can use finesse measurements of a MOTIRR with well-polished TIR surfaces to obtain upper limits for the bulk loss at any wavelength.

ACKNOWLEDGMENTS

We are indebted to J. Vrhel for the skillful fabrication of the MOTIRR's and to S. T. Yang for assistance during the early stages of this study, and we thank A. Sizmann, K. Fiedler, R. Paschotta, and R. C. Eckardt for helpful discussions. This research was supported by National Science Foundation grant NSF PHY 92-15157.

*Present address, Fakultät für Physik, Universität Konstanz, P.O. Box 5560, D-78434 Konstanz, Germany.

REFERENCES AND NOTES

1. W. J. Kozlovsky, C. D. Nabors, R. C. Eckardt, and R. L. Byer, "Monolithic MgO:$LiNbO_3$ doubly resonant optical parametric oscillator pumped by a frequency-doubled diode-laser-pumped Nd:YAG laser," Opt. Lett. **14,** 66–68 (1989).
2. C. D. Nabors, R. C. Eckardt, W. J. Kozlovsky, and R. L. Byer, "Efficient, single-axial-mode operation of a monolithic MgO:$LiNbO_3$ optical parametric oscillator," Opt. Lett. **14,** 1134–1136 (1989).
3. S. Schiller, I. I. Yu, M. M. Fejer, and R. L. Byer, "Fused-silica monolithic total-internal-reflection resonator," Opt. Lett. **17,** 378–380 (1992).
4. P. Beckmann and A. Spizzichino, *The Scattering of Electromagnetic Waves from Rough Surfaces* (Macmillan, New York, 1963).
5. J. M. Bennett, V. Elings, and K. Kjoller, "Precision metrology for studying optical surfaces," Opt. Photon. News **2**(5), 14–18 (1991).
6. S. Schiller, "Principles and applications of optical monolithic total-internal-reflection resonators," Ph.D. dissertation, Ginzton Laboratory Rep. No. 5069 (Stanford University, Stanford, Calif., 1993).
7. K. Fiedler, S. Schiller, R. Paschotta, P. Kürz, and J. Mlynek, "Highly efficient frequency doubling with a doubly resonant monolithic total internal reflection resonator," Opt. Lett. (to be published).
8. P. D. Drummond, K. J. McNeil, and D. F. Walls, "Non-equilibrium transitions in sub/second harmonic generation. I. Semiclassical theory," Opt. Acta **27,** 321–335 (1980).
9. C. M. Savage and D. F. Walls, "Optical chaos in second-harmonic generation," Opt. Acta **30,** 557–561 (1983).
10. M. J. Collett and D. F. Walls, "Squeezing spectra for nonlinear optical systems," Phys. Rev. A **32,** 2887–2892 (1985).
11. H. J. Kimble and J. L. Hall, "Intracavity frequency doubling for the generation of squeezed states of light," in *Quantum Optics IV,* J. D. Harvey and D. F. Walls, eds. (Springer-Verlag, Berlin, 1986), pp. 58–69.
12. S. F. Pereira, M. Xiao, H. J. Kimble, and J. L. Hall, "Generation of squeezed light by intracavity frequency doubling," Phys. Rev. A **38,** 4931–4934 (1988).
13. A. Sizmann, R. J. Horowicz, G. Wagner, and G. Leuchs, "Observation of amplitude squeezing of the up-converted mode in second harmonic generation," Opt. Commun. **80,** 138–142 (1990).
14. P. Kürz, R. Paschotta, K. Fiedler, A. Sizmann, G. Leuchs, and J. Mlynek, "Squeezing by second-harmonic generation in a monolithic resonator," Appl. Phys. B **55,** 216–225 (1992).
15. C. Zimmermann, R. Kallenbach, T. W. Hänsch, and

J. Sandberg, "Doubly-resonant second-harmonic generation in β-barium borate," Opt. Commun. **71,** 229–234 (1989).
16. C. Zimmermann, T. W. Hänsch, R. L. Byer, S. O'Brien, and D. Welch, "Second harmonic generation at 972 nm using a distributed Bragg reflection semiconductor laser," Appl. Phys. Lett. **61,** 2741–2743 (1992).
17. A. Yariv and W. H. Louisell, "Theory of the optical parametric oscillator," IEEE J. Quantum Electron. **QE-2,** 418–424 (1966); for a review see W. Brunner and H. Paul, "Theory of optical parametric amplification and oscillation," in *Progress in Optics,* E. Wolf, ed. (North-Holland, Amsterdam, 1977), Vol. 15, pp. 1–75.
18. J. Mertz, T. Debuisschert, A. Heidmann, C. Fabre, and E. Giacobino, "Improvements in the observed intensity correlation of optical parametric oscillator twin beams," Opt. Lett. **16,** 1234–1236 (1991).
19. F. G. Colville, A. J. Henderson, M. J. Padgett, J. Zhang, and M. H. Dunn, "Continuous-wave parametric oscillation in lithium triborate," Opt. Lett. **18,** 205–207 (1993).
20. A. Siegman, *Lasers* (University Science, Mill Valley, Calif., 1986).
21. R. C. Eckardt, C. D. Nabors, W. J. Kozlovsky, and R. L. Byer, "Optical parametric oscillator frequency tuning and control," J. Opt. Soc. Am. B **8,** 646–667 (1991).
22. These equations are also applicable to the calculation of the external conversion efficiency of a DR-SHG device that employs dedicated out-coupling of the harmonic (see Ref. 7).
23. R. C. Eckardt, H. Masuda, Y. X. Fan, and R. L. Byer, "Absolute and relative nonlinear optical coefficients of KDP, KD*P, BaB_2O_4, $LiIO_3$, MgO:$LiNbO_3$, and KTP measured by phase-matched second-harmonic generation," IEEE J. Quantum Electron. **26,** 922–933 (1990).
24. W. J. Kozlovsky, C. D. Nabors, and R. L. Byer, "Efficient second harmonic generation of a diode-laser-pumped Nd:YAG laser using monolithic MgO:$LiNbO_3$ external resonant cavities," IEEE J. Quantum Electron. **24,** 913–919 (1988).
25. G. D. Boyd and D. A. Kleinman, "Parametric interaction of focused Gaussian light beams," J. Appl. Phys. **39,** 3597–3638 (1968).
26. L.-A. Wu and H. J. Kimble, "Interference effects in second-harmonic generation within an optical cavity," J. Opt. Soc. Am. B **2,** 697–703 (1985).
27. T. Debuisschert, A. Sizmann, E. Giacobino, and C. Fabre, "Type-II continuous-wave optical parametric oscillators: oscillation and frequency-tuning characteristics," J. Opt. Soc. Am. B **10,** 1668–1680 (1993).
28. R. W. P. Drever, J. L. Hall, F. V. Kowalski, J. Hough, G. M. Ford, A. J. Munley, and H. Ward, "Laser phase and frequency stabilization using an optical resonator," Appl. Phys. B **31,** 97–105 (1983).
29. D. Serkland, Department of Applied Physics, Stanford University, Stanford, Calif. 94305 (personal communication, 1991).
30. S. Lin, B. Wu, F. Xie, and C. Chen, "Phase-matching retracing behavior: new features in LiB_3O_5," Appl. Phys. Lett. **59,** 1541–1543 (1991).
31. W. P. Risk and W. J. Kozlovsky, "Efficient generation of blue light by doubly resonant sum-frequency mixing in a monolithic KTP resonator," Opt. Lett. **17,** 707–709 (1992).
32. S. T. Yang, R. C. Eckardt, and R. L. Byer, "Continuous-wave singly resonant optical parametric resonator pumped by a single-frequency resonantly doubled Nd:YAG laser," Opt. Lett. **18,** 971–973 (1993).
33. L. A. Lugiato, C. Oldano, C. Fabre, E. Giacobino, and R. J. Horowicz, "Bistability, self-pulsing and chaos in optical parametric oscillators," Nuovo Cimento D **10,** 959–977 (1988).